A Combined Experimental and Theoretical Study on the Formation of Ag Filaments on β-Ag_2MoO_4 Induced by Electron Irradiation

Juan Andrés[*1], *Mateus M. Ferrer*[2] , *Lourdes Gracia*[1,3], *Armando Beltran*[1], *Valeria M. Longo*[4], *Guilherme H. Cruvinel*[4], *Ricardo L. Tranquilin*[2] *and Elson Longo*[3]

[1]Departament de Química Física i Analítica, Universitat Jaume I, 12071, Castelló de la Plana, Spain.

[2]INCTMN-UFSCar, Universidade Federal de São Carlos, P.O. Box 676, 13565-905 São Carlos, SP, Brazil

[3]INCTMN-UNESP, Universidade Estadual Paulista, P.O. Box 355, CEP. 14801-907 Araraquara, SP, Brazil

[4]INCTMN-USP, Universidade de São Paulo, Instituto de Física de São Carlos, 13560-970, São Carlos, SP, Brazil

*Corresponding author: andres@qfa.uji.es

Keywords: β-Ag_2MoO_4, semiconductor, electron beam, topological analysis, Ag filaments.

Abstract

A combined experimental and theoretical study is presented to understand **the novel** observed nucleation and early evolution of Ag filaments on β−Ag_2MoO_4 crystals, driven by an accelerated electron beam from an electronic microscope under high *vacuum*. The growth process, chemical composition and the element distribution in these filaments were analyzed in depth at the nanoscale level using field emission scanning electron microscopy (FE-SEM) and transmission electron microscopy (TEM) with

energy dispersive spectroscopy (EDS) characterization. To complement experimental results, chemical stability, structural and electronic aspects have been studied systematically using first-principles electronic structure theory within a QTAIM framework. The Ag nucleation and formation on β-Ag_2MoO_4 is a result of structural and electronic changes of the AgO_4 tetrahedral cluster as a constituent building block of β-Ag_2MoO_4, consistent with Ag metallic formation. The formation of Ag filament transforms the β-Ag_2MoO_4 semiconductor from *n* to *p* type concomitant with the appearance of Ag defects.

1. Introduction

Metal tungstates and molybdates form a family of multicomponent metal oxide compounds, and many studies have been made regarding their interesting structures, intriguing physical and chemical properties, as well as a wide range of applications in photoluminescence, optical fibers, scintillator materials, photochromism, humidity sensors, multiferroic materials, and catalysts.[1-19]

One member of the molybdate family, silver molybdate (Ag_2MoO_4) has been a target of intense investigation for its chemical stability at elevated temperatures and subsequent high-temperature lubricating properties[20]as well as its potential applications in electrochemical devices and gas-sensing,[20-24]and in surface enhanced Raman scattering techniques.[23,25] Several studies have been made to obtain Ag_2MoO_4 based materials as flower-like,[26] nanoparticles[21] and wire-like nanostructures.[22]Low dimensional Ag_2MoO_4 nanostructures have been obtained by Nagaraju *et al.* who reported the synthesis of

nanorods/nanowires/multipods and the photoluminescence of microrods;[27] while Feng et al. have been synthetized as ultra long orthorhombic silver trimolybdate nanowires[28]. Qian et al.[29]have reported the microwave-assisted hydrothermal synthesis of cube-like Ag-Ag_2MoO_4 with visible-light photocatalytic activity. Bao et al.[30]reported on a room-temperature synthesis of Ag nanoparticles decorated with silver molybdate nanowires using a solution-based chemical reaction method. Fodjo et al.[25]have published a facile hydrothermal technique to synthesize Ag_2MoO_4 at relatively low temperatures (80 ºC and 20 ºC). Tang et al.[31]have obtained $Ag_2Mo_2O_7$/chitin composite gel-membranes which were fabricated incorporating $Ag_2Mo_2O_7$ in the regenerated chitin gel-membranes via a green pathway. Cheng *et al*.[22] studied photoswitches of one-dimensional Ag_2MO_4 (M = Cr, Mo, and W) and noticed the formation of silver nanoparticles at the surface of Ag_2MoO_4 under electron beam irradiation, as already previously reported during TEM observation of other silver nanowires.[32]

The ability of chemists and physicists to interact with atoms, molecules, and solids at the quantum level; and the spatial scales of atoms and chemical bonds and on temporal scales of electron and nuclear motion has gained increasing sophistication through the development of precise photon and electron probes. In particular, electron probes have precise spatial resolution, which has enabled imaging of single atoms and atomic lattice contrast on surfaces and in solids. Scanning electron microscopy (SEM), scanning transmission electron microscopy (STEM), and transmission electron microscopy (TEM) are well recognized techniques that provide unique capabilities for *in situ* imaging and control of nanoscale phenomena.[33-37]

In recent years, papers on monitoring local structural and electronic changes generated by the electron beam within TEM have been started to appear, and TEM is a very powerful tool for the observation, fabrication and manipulation of nanostructures with the advantages of precise nanoscale control,[38,39] in which high energy electrons transmit through the specimen and provide useful electronic structure information of the samples based on a variety of electron-solid interactions.[40]Applying this technique, novel phenomena have been discovered in the process of TEM observation, such as nanoscale phase/shape transformation,[41]inorganic nanostructure modification,[42]colloid nanocrystal growth and self assembly,[36,43-47]lithium encapsulation and release in LiCl nanoshells and nanotubes,[48]nanostructure fabrication,[49]coalescence,[50]nanoscale crystallization and some growth processes which occur only in the beam's presence.[36,44,46,47,51,52]Different studies have quantified the role of the electron beam in affecting the chemical reactions being characterized.[44,52]

In particular, electron beam irradiation allows the preparation of noble and transition metal nanoparticles;[43,53]Pattabi *et al.* have synthesized silver nanoparticles with enhanced antibacterial activity by using electron beam irradiation.[54]During imaging, the electron beam interacts with the sample causing a novel phenomenon that occurs only in the beam´s presence. In particular, an accurate understanding of the interactions between the electron beam and the material is essential to account for, suppress, and exploit the beam effects. First principle calculations are essential in supporting the experimental observation to provide a deeper understanding of atomic and electronic structure that is already being exploited to explain their innovative properties and allow efficient exploration of new materials. In this context, very recently, the formation of Ag filaments

on α-Ag_2WO_4 induced by electron irradiation[55] and their bactericidal[56] and photoluminescent applications,[57]as well their application as an efficient ozone sensor have been reported.[58]

The crystal structure Ag_2MoO_4 obtained by Wyckoff[59]can be found in two forms: α-Ag_2MoO_4 has a tetragonal structure while β-Ag_2MoO_4 is cubic with a spinel structure.[59-61] The α-phase irreversibly transforms to the most stable β-phase upon heating above ambient temperature. Arora *et al.*[60]have studied the behavior of the cubic spinel phase of Ag_2MoO_4 at high pressure as characterized by X-ray diffraction and Raman spectroscopy, and, in this context, our group has studied the effect of pressure on β-Ag_2MoO_4[62]as a continuation of previous articles on the $MgAl_2O_4$ normal spinel and Zn_2SnO_4 inverse spinel structures.[63,64] Very recently, we have investigated a correlation between theoretical calculations and experimental data to explain the electronic structure and optical properties of β-Ag_2MoO_4 microcrystals.[65]

Due to the novelty associated to the observed nucleation and early evolution of Ag filaments on β–Ag_2MoO_4 crystals, driven by an accelerated electron beam from an electronic microscope under high *vacuum*. Here, we report on a comprehensive and combined experimental and theoretical work to understand the observed nucleation and early evolution of Ag filaments on β-Ag_2MoO_4 crystals, driven by an accelerated electron beam from an electronic microscope under high *vacuum*. We have studied the geometric and electronic structure of β-Ag_2MoO_4, and have derived a mechanism sequence using electron irradiation as relevant to early events for the formation and growth of Ag filaments from AgO_6 and MoO_4 clusters, as constituent polyhedra of β-Ag_2MoO_4. Quantum theory of atoms in molecules (QTAIM) developed by Bader and

collaborators[66-68]allows the analysis of the experimental or theoretical electron density distribution, $\rho(r)$, in a solid, and the study of properties of $\rho(r)$ to reveal the bonding interactions in the crystal system, and the nature of these interactions. The electronic charge of each atom is evaluated using the Bader charge analysis within the QTAIM framework, which is a way of dividing molecules or solids into atoms based on electronic charge density. These computations envisaged in this study are thought to answer the questions: What happens with the electron excess as it approaches the surface and bulk of β–Ag_2MoO_4? How are the electrons distributed in this material and how can it is related with the structural and electronic evolution? How does the strength of the Ag-O and Mo-O bonds change after electron irradiation β–Ag_2MoO_4? We shall discuss how the analysis, provided from both experimental and theoretical results, of the structural and electronic structure of β-Ag_2MoO_4 allows us to explain the Ag nucleation process. The discussion will address the details of image acquisition and analysis and will provide a guide to interpret experimental results.

2. Results and discussion

Figure 1 shows the XRD patterns of β-Ag_2MoO_4 which were prepared using the microwave-assisted hydrothermal method. All of the diffraction peaks of samples can be indexed as cubic structure without any deleterious phases, and with a space group of ($Fd\bar{3}m$) and point-group symmetry (O_h^7) and are in agreement with the standard values of Inorganic Crystal Structure Data (ICSD) base no. 28891[61]

Figure 2 shows the Raman spectrum of the as-prepared β–Ag_2MoO_4 between 100 -1000 cm^{-1}. It is possible to verify the presence of four Raman active modes which indicates the structural order at short-range. The active Raman mode (E_g) located at 279 cm^{-1} is corresponds to the external structure vibrations which correspond to octahedral [AgO_6] clusters, while Raman mode (F_{2g}) found at 354 cm^{-1} is related to the torsional vibration of the [O–Mo–O] bonds present in the tetrahedral [MoO_4] clusters. Finally, the active Raman mode (A_{1g}) found at 873 cm^{-1} corresponds to the symmetric stretching vibration of the [←O←Mo→O→] bonds clusters present in the tetrahedral [MoO_4] clusters.[23,65]

Figure 3 shows a time-resolved series of FE-SEM images obtained under high vacuum (1×10^{-5} Pa) during the growth of Ag filaments stimulated by the electron beam on the β–Ag_2MoO_4 surface. Figure 3 a shows a FE-SEM image of the crystals that were acquired after a rapid approach and focus adjustment (time zero). At this point, the image reveals a small amount of Ag on the surface. Figure 3 b shows that after 2 min of exposure to a 30 kV electron beam, the particle shows some regions with Ag on the surface. It is interesting to notethat the modifications, even small, occur after a few seconds of exposure. After 6 min of exposure, Figure 3 d, the metallic Ag seems to reach a limit point of growth. Further information, a short video **(video S1)** of the Ag growth is in the Supplementary Information.

Figure 4 illustrates the TEM images with EDS characterization. Results of the composition are shown in Table 1. Therefore the end of the region that emerged due to the electron exposure (point 1) confirmed the composition of 100% of Ag in relation of Mo. Furthermore, it is possible to see the crystallographic planes revealing the Ag

crystallinity. The region near the interface and inside the particles, points 2 and 3, consisted of about 64% of Mo to 36% of Ag. These results reinforce the fact that the Ag atoms come from the interior deep regions of the particles. This behavior provokes the presence of Ag defects inside β-Ag_2MoO_4 material and this semiconductor changes from *n* to *p* type.

Figure 5 a) shows the conventional cubic unit cell containing 8 formula units. Mo ions (grey atoms) occupy tetrahedral 8a sites while Ag ions (blue atoms) reside at the octahedral 16d position. Oxygen atoms (red atoms) stay at 32e positions. Arora et al.[60]performed powder XRD measurements at ambient pressure obtaining a single-phase material with a lattice parameter of 9.313 Å. Our calculations at ambient pressure yield a lattice parameter of 9.427 Å which is only 1.2% greater than the experimental value.[62] The primitive unit cell is depicted in Figure 5 b), with only 2 formula units.

In sense to understand the quantum phenomenon observed experimentally of electron absorption we introduced electrons, separately, up to ten in the cluster constituent of the cubic unit cell of β-Ag_2MoO_4. The values for the distances Ag-O and Mo-O as a function of the number of electrons, N, are shown in **Figure 6**. In the case of Ag-O distances there is a pronounced increase with the addition of electrons.

An analysis of the results presented in **Figure 7** shows that the Ag atoms of the [AgO_6] clusters are the more prone to be reduced. At N=4, practically all Ag atoms are reduced whereas, there is a minor decrease of the electron density is sensed for Mo atoms (that form [MoO_4] clusters) (a decrease of 0.2 units at N=4). Therefore, the electron excess imposed in the material is transferred from one cluster to another through the

lattice network and the Ag formation process involves [AgO_6] adjacent clusters, and to a minor extent the [MoO_4] clusters.

Bond critical points densities and its Laplacian: The calculations of the charge density, ρ_{bcp}, at the (3,-1) bond critical points (BCP) as well as its Laplacian, $\nabla^2\rho_{bcp}$, in Ag-O bonds for [AgO_6] units are presented in **Table 2**. The effect of adding electrons to the material produces striking differences in the values of the Laplacian and charge density at the (3,-1) BCP. Thus, it is worth noting that the Ag-O bonds considerably reduce their Laplacian and charge density values as the number of electrons are added indicating that these bonds become less strong in favor of the formationof metallic Ag.

3. Conclusions

The dynamics and the state properties of excess electrons, provided by an electron beam of TEM, have attracted widespread interest due to the fundamental importance of this process in physics, chemistry, and biology. The electron beam irradiation in TEM provokes the synthesis of nanomaterials and investigating their morphology, structure, and chemical transformation, which is of importance for the development of novel nanostructures, especially for those that cannot be obtained using conventional chemical and physical methods.

Electron–material interactions offer an alternative approach to control the electronic structure and thus the chemical and physical properties, and the corresponding activities. In particular, the addition of electrons generated large change in the charge

density e resulting in bond modifications. As a consequence, a wide range of different chemistries can be initiated by electron–material interactions.

We report the *in situ* growth of Ag on β-Ag_2MoO_4, **never observed before,** by electron beam irradiation, and this work provides a fundamental perspective on the chemistry initiated by electrons on β–Ag_2MoO_4 via a non-classical mechanism. This insight is relevant to apparently unrelated topics such as surface functionalisation or electron beam induced deposition processes. Moreover, mutual awareness of the common concepts of these different fields will also help to solidify the broader understanding of electron-initiated process because each field, and others, can provide examples that reveal principles of common interest. Electron-initiated chemistry therefore remains an active and dynamic research area and many more interesting discoveries and applications can be expected.

The present study communicates intimate details on the internal processes and these findings raise fundamental questions about the physical nature of this phenomenon itself. The results derived from the present study are based on the information provided by the joint analysis of experimental and theoretical work to provide a deeper insight and understanding of increasingly complex functional materials, and can be considered as a clear example of a complex modeling paradigm as was introduced by Billinge and Levin.[75]

4. Experimental procedure

4.1. Synthesis of β-Ag_2MoO_4

β-Ag_2MoO_4 microcrystals were prepared at room temperatures without the use of any surfactant by a simple precipitation method. The typical β-Ag_2MoO_4 crystals synthesis procedure is described as follows: 1×10^{-3}mols of molybdate sodium dihydrate ($Na_2MoO_4.2H_2O$; 99.5% purity, Sigma-Aldrich) and 2×10^{-3}mols of silver nitrate ($AgNO_3$; 99.8% purity, Sigma-Aldrich) were each separately dissolved in 50 mL of deionized water. The silver solution was dripped into the molybdate solution under stirring. The resulting suspensions were washed with deionized water several times to remove remaining ions and dried at 60ºC for 12 h.

4.2. Experimental characterizations of β-Ag_2MoO_4

The β-Ag_2MoO_4 crystals were structurally characterized by X-ray diffraction (XRD) patterns using a diffractometer model LabX XRD-6000 (Shimadzu®, Japan) with Cu-Kα radiation (λ = 1.5406 Å) in the 2θ range from 20° to 80° in the normal routine with a scanning velocity of 1°/min. Micro-Raman measurements were recorded using the (Horiba; Jobin-Yvon, France) model LabRAM HR 800 mm.

The shapes, sizes, visualization of Ag filaments and element distribution of the β-Ag_2MoO_4 microcrystals were observed with a field-emission scanning electron microscope (FEG-SEM) model Supra 35-VP, Carl Zeiss, Germany operated at 20 kV, and transmission electron microscopy (TEM) operating at 200 KV, and Electron Dispersion Spectroscopy (EDS); model Tecnai G2TF20, FEI.

4.3.Theoretical calculations

First-principles total-energy calculations were carried out within the periodic density-functional-theory (DFT) framework using the VASP program.[69,70] The Kohn-Sham equations have been solved by means of the Perdew, Burke, and Ernzerhof exchange-correlation functional,[69] and the electron-ion interaction as described by the projector-augmented-wave pseudopotentials.[71,72] Due to the well known limitations of standard DFT in describing the electronic structure of "strongly-correlated" compounds, a correction to the PBE wavefunctions are adopted (PBE+U) with the inclusion of a repulsive on-site Coulomb interaction U following the methodof Dudarev et al.[73]. Eventually the value of the Hubbard parameter was tested and a value of U = 6 eV was used. The plane-wave expansion was truncated at a cut-off energy of 400 eV and the Brillouin zones have been sampled through Monkhorst-Pack special *k*-points grids that as sure geometrical and energetic convergence for the Ag_2MoO_4 structures considered in this study. The keyword NELECT has been used in order to increase the number of electrons in the bulk structure, and all the crystal structures are optimized simultaneously on both the volume of the unit-cell and the atomic positions.The relationship between charge density topology and elements of molecular structure and bonding was noted by Bader.[66,74]This relationship, Bader's quantum theory of atoms in molecules (QTAIM),[66-68]is now a well-recognized tool used to analyze electron density, to describe interatomic interactions, and to rationalize chemical bonding. The different strong and weak interactions between two atoms can be determined unequivocally from QTAIM calculations. According to the standard QTAIM framework, concepts such as (3,-1) bond

critical points (BCPs), their respective bond paths (BPs), and $L(r) = -\nabla^2\rho(r)$ maps can be analyzed to reveal the nature of these interactions. A BCP serves as the origin of gradient lines of the electron density that define the interatomic surface or zero-flux surface—a surface that unambiguously defines the boundary between the two atoms and identifies the atomic basin, i.e., the electron density "belonging" to a specific atom.

Acknowledgments

The authors are grateful to Prometeo/2009/053 (GeneralitatValenciana), Ministerio de Economia y Competitividad (Spain), CTQ2012-36253-C03-02, Spanish Brazilian program (PHB2009-0065-PC), FAPESP (Project 2013/07296-2 and 2012/14468-1), INCTMN/FAPESP (Project 2008/57872-1), INCTMN/CNPq (Project 573636/2008-7 and Grant 150753/2013-6) for financially supporting this research. We also acknowledge the ServeiInformática, UniversitatJaume I, for the generous allotment of computer time.

(1) V. B. Mikhailik, H. Kraus, G. Miller, M. S. Mykhaylyk, D. Wahl, *J. Appl. Phys.* **2005**, *97*, 083523.

(2) F. Amano, A. Yamakata, K. Nogami, M. Osawa, B. Ohtani, *J. Am. Chem. Soc.* **2008**, *130*, 17650.

(3) K. Fukuda, K. Akatsuka, Y. Ebina, R. Ma, K. Takada, I. Nakai, T. Sasaki, *Acs Nano* **2008**, *2*, 1689.

(4) M. Shang, W. Z. Wang, H. L. Xu, *Cryst. Growth Des.* **2009**, *9*, 991.

(5) S. Y. Song, Y. Zhang, Y. Xing, C. Wang, J. Feng, W. D. Shi, G. L. Zheng, H. J. Zhang, *Adv. Funct. Mater.* **2008**, *18*, 2328.

(6) Y. G. Su, L. P. Li, G. S. Li, *Chem. Mater.* **2008**, *20*, 6060.

(7) D. Ye, D. Z. Li, W. J. Zhang, M. Sun, Y. Hu, Y. F. Zhang, X. Z. Fu, *J. Phys. Chem. C* **2008**, *112*, 17351.

(8) L. W. Zhang, Y. J. Wang, H. Y. Cheng, W. Q. Yao, Y. F. Zhu, *Adv. Mater.* **2009**, *21*, 1286.

(9) Y. Zhao, Y. Xie, X. Zhu, S. Yan, S. X. Wang, *Chem. Eur. J.* **2008**, *14*, 1601.

(10) L. Zhou, W. Z. Wang, H. L. Xu, S. M. Sun, *Cryst. Growth Des.* **2008**, *8*, 3595.

(11) Y. X. Zhou, Q. Zhang, J. Y. Gong, S. H. Yu, *J. Phys. Chem. C* **2008**, *112*, 13383.

(12) L. Gracia, V. M. Longo, L. S. Cavalcante, A. Beltran, W. Avansi, M. S. Li, V. R. Mastelaro, J. A. Varela, E. Longo, J. Andres, *J. Appl. Phys.* **2011**, *110*, 043501.

(13) V. M. Longo, L. Gracia, D. G. Stroppa, L. S. Cavalcante, M. Orlandi, A. J. Ramirez, E. R. Leite, J. Andres, A. Beltran, J. A. Varela, E. Longo, *J. Phys. Chem. C* **2011**, *115*, 20113.

(14) E. Orhan, F. M. Pontes, C. D. Pinheiro, E. Longo, P. S. Pizani, J. A. Varela, E. R. Leite, T. M. Boschi, A. Beltran, J. Andres, *J. Eur. Ceram. Soc.* **2005**, *25*, 2337.

(15) N. M. Batra, S. K. Arora, T. Mathews, *J. Mater. Sci. Lett.* **1988**, *7*, 254.

(16) M. R. D. Bomio, R. L. Tranquilin, F. V. Motta, C. A. Paskocimas, R. M. Nascimento, L. Gracia, J. Andres, E. Longo, *J. Phys. Chem. C* **2013**, *117*, 21382.

(17) W. S. Cho, M. Yashima, M. Kakihana, A. Kudo, T. Sakata, M. Yoshimura, *J. Am. Ceram. Soc.* **1997**, *80*, 765.

(18) F. Lei, B. Yan, H. H. Chen, Q. Zhang, J. T. Zhao, *Cryst. Growth Des.* **2009**, *9*, 3730.

(19) J. C. Sczancoski, L. S. Cavalcante, N. L. Marana, R. O. da Silva, R. L. Tranquilin, M. R. Joya, P. S. Pizani, J. A. Varela, J. R. Sambrano, M. S. Li, E. Longo, J. Andres, *Curr. Appl. Phys.* **2010**, *10*, 614.

(20) W. Gulbinski, T. Suszko, *Wear* **2006**, *261*, 867.

(21) S. Bhattacharya, A. Ghosh, *Phys. Rev. B* **2007**, *75*, 092103.

(22) L. Cheng, Q. Shao, M. W. Shao, X. W. Wei, Z. C. Wu, *J. Phys. Chem. C* **2009**, *113*, 1764.

(23) E. Y. Liu, W. Z. Wang, Y. M. Gao, J. H. Jia, *Tribol. Lett.* **2012**, *47*, 21.

(24) A. Sanson, F. Rocca, C. Armellini, S. Ahmed, R. Grisenti, *J. Non-Cryst. Solids* **2008**, *354*, 94.

(25) E. K. Fodjo, D.-W. Li, N. P. Marius, T. Albert, Y.-T. Long, *J. Mater. Chem. A* **2013**, *1*, 2558.

(26) D. P. Singh, B. Sirota, S. Talpatra, P. Kohli, C. Rebholz, S. M. Aouadi, *J. Nanopart. Res.* **2012**, *14*, 781.

(27) G. Nagaraju, G. T. Chandrappa, J. Livage, *Bull. Mater. Sci.* **2008**, *31*, 367.

(28) M. Feng, M. Zhang, J.-M. Song, X.-G. Li, S.-H. Yu, *Acs Nano* **2011**, *5*, 6726.

(29) L. Z. Qian, C. X.Tai, X. Z. Ling, *Sci. China Chem.* **2013**, *56*, 443

(30) Z. Y. Bao, D. Y. Lei, J. Dai, Y. Wu, *Appl. Surf. Sci.* **2013**, *287*, 404.

(31) H. Tang, A. Lu, L. Li, W. Zhou, Z. Xie, L. Zhang, *Chem. Eng. J.* **2013**, *234*, 124.

(32) X. J. Cui, S. H. Yu, L. L. Li, L. Biao, H. B. Li, M. S. Mo, X. M. Liu, *Chem. Eur. J.* **2004**, *10*, 218.

(33) N. de Jonge, F. M. Ross, *Nat. Nanotechn.* **2011**, *6*, 695.

(34) R. F. Egerton, P. Li, M. Malac, *Micron* **2004**, *35*, 399.

(35) L. R. Parent, D. B. Robinson, T. J. Woehl, W. D. Ristenpart, J. E. Evans, N. D. Browning, I. Arslan, *Acs Nano* **2012**, *6*, 3589.

(36) T. J. Woehl, J. E. Evans, L. Arslan, W. D. Ristenpart, N. D. Browning, *Acs Nano* **2012**, *6*, 8599.

(37) T. J. Woehl, K. L. Jungjohann, J. E. Evans, I. Arslan, W. D. Ristenpart, N. D. Browning, *Ultramicroscopy* **2013**, *127*, 53.

(38) D. Tham, C. Y. Nam, J. E. Fischer, *Adv. Mater.* **2006**, *18*, 290.

(39) M. Y. Yen, C. W. Chiu, F. R. Chen, J. J. Kai, C. Y. Lee, H. T. Chiu, *Langmuir* **2004**, *20*, 279.

(40) Y. Xu, L. Shi, X. Zhang, K. Wong, Q. Li, *Micron* **2011**, *42*, 290.

(41) A. H. Latham, M. E. Williams, *Langmuir* **2008**, *24*, 14195.

(42) J. H. Warner, *Adv. Mater.* **2008**, *20*, 784.

(43) J. U. Kim, S. H. Cha, K. Shin, J. Y. Jho, J. C. Lee, *J. Am. Chem. Soc.* **2005**, *127*, 9962.

(44) J. E. Evans, K. L. Jungjohann, N. D. Browning, I. Arslan, *Nano Lett.* **2011**, *11*, 2809.

(45) J. Park, H. Zheng, W. C. Lee, P. L. Geissler, E. Rabani, A. P. Alivisatos, *Acs Nano* **2012**, *6*, 2078.

(46) J. M. Yuk, J. Park, P. Ercius, K. Kim, D. J. Hellebusch, M. F. Crommie, J. Y. Lee, A. Zettl, A. P. Alivisatos, *Sci.* **2012**, *336*, 61.

(47) H. Zheng, R. K. Smith, Y.-w. Jun, C. Kisielowski, U. Dahmen, A. P. Alivisatos, *Sci.* **2009**, *324*, 1309.

(48) W. Neng, M. Martini, W.-n. Su, X. Ling, L.-t. Sun, Y.-t. Shen, *Crystengcomm* **2013**, *15*, 7872.

(49) D. Wan, M. Matteo, W. N. Su, L. Xu, L. T. Sun, Y. T. Shen, *CrystEngComm* **2013**, *15*, 7872.

(50) Y. Liu, X.-M. Lin, Y. Sun, T. Rajh, *J. Am. Chem. Soc.* **2013**, *135*, 3764.

(51) H.-G. Liao, L. Cui, S. Whitelam, H. Zheng, *Sci.* **2012**, *336*, 1011.

(52) K. W. Noh, Y. Liu, L. Sun, S. J. Dillon, *Ultramicroscopy* **2012**, *116*, 34.

(53) S. Sepulveda-Guzman, N. Elizondo-Villarreal, D. F. A. Torres-Castro, X. Gao, J. P. Zhou, M. Jose-Yacaman, *Nanotechn.* **2007**, *18*, 335604.

(54) R. M. Pattabi, K. R. Sridhar, S. Gopakumar, B. Vinayachandra, M. Pattabi, *Int. J. Nanoparticles* **2010**, *3*, 53.

(55) E. Longo, L. S. Cavalcante, D. P. Volanti, A. F. Gouveia, V. M. Longo, J. A. Varela, M. O. Orlandi, J. Andres, *Sci. Rep.* **2013**, *3*, 1676.

(56) V. M. Longo, C. C. D. Foggi, M. M. Ferrer, A. F. Gouveia, R. S. André, W. Avansi, C. E. Vergani, A. L. Machado, J. Andrés, L. S. Cavalcante, A. C. Hernandes, E. Longo, *J. Phys. Chem. A* **2014** *doi:10.1021/jp410564p*.

(57) E. Longo, D. P. Volanti, V. R. M. Longo, L. Gracia, I. A. C. Nogueira, M. A. P. Almeida, A. N. Pinheiro, M. M. Ferrer, L. S. Cavalcante, J. Andrés, *J. Phys. Chem. C* **2014**, *doi:10.1021/jp408167v*.

(58) L. F. da Silva, A. C. Catto, W. J. Avansi, L. S. Cavalcante; J. Andrés, K. Aguir, V. R. Mastelaro, E. Longo, *Nanoscale* **2014**, *6*, 4058.

(59) R. W. G. Wyckoff, *J. Am. Chem. Soc.* **1922**, *44*, 1994.

(60) A. K. Arora, R. Nithya, S. Misra, T. Yagi, *J. Solid State Chem.* **2012**, *196*, 391.

(61) J. Donohue, W. Shand, *J. Am. Chem. Soc.* **1947**, *69*, 222.

(62) A. Beltran, L. Gracia, E. Longo, J. Andrés, *J. Phys. Chem. C* **2014**, *118*, 3724.

(63) L. Gracia, A. Beltran, J. Andres, *J. Phys. Chem. C* **2011**, *115*, 7740.

(64) L. Gracia, A. Beltran, J. Andres, R. Franco, J. M. Recio, *Phys. Rev. B* **2002**, *66*, 224114.

(65) A. F. Gouveia, J. C. Sczancoski, M. M. Ferrer, A. S. Lima, M. R. M. C. Santos, M. S. Li, R. S. Santos, E. Longo, L. S. Cavalcante, *Inorg. Chem.* **2014**, *doi:10.1021/ic500335x.*

(66) R. F. W. Bader, *Atoms in molecules : a quantum theory*; Clarendon Press Oxford New York, **1990**.

(67) C. F. Matta, R. J. Boyd, *The quantum theory of atoms in molecules*; Wiley-VCH: Weinheim, **2007**.

(68) P. L. A. Popelier, *Atoms in molecules : an introduction*; Prentice Hall: Harlow, **2000**.

(69) G. Kresse, J. Furthmuller, *Comput. Mater. Sci.* **1996**, *6*, 15.

(70) G. Kresse, J. Hafner, *Phys. Rev. B* **1994**, *49*, 14251.

(71) G. Kresse, D. Joubert, *Phys. Rev. B* **1999**, *59*, 1758.

(72) J. P. Perdew, K. Burke, M. Ernzerhof, *Phys. Rev. Lett.* **1996**, *77*, 3865.

(73) S. L. Dudarev, G. A. Botton, S. Y. Savrasov, C. J. Humphreys, A. P. Sutton, *Phys. Rev. B* **1998**, *57*, 1505.

(74) P. Hohenberg, W. Kohn, *Phys. Rev. B***1964**, *136*, B864.

(75) S. J. L. Billinge, I. Levin, *Sci.* **2007**, *316*, 561.

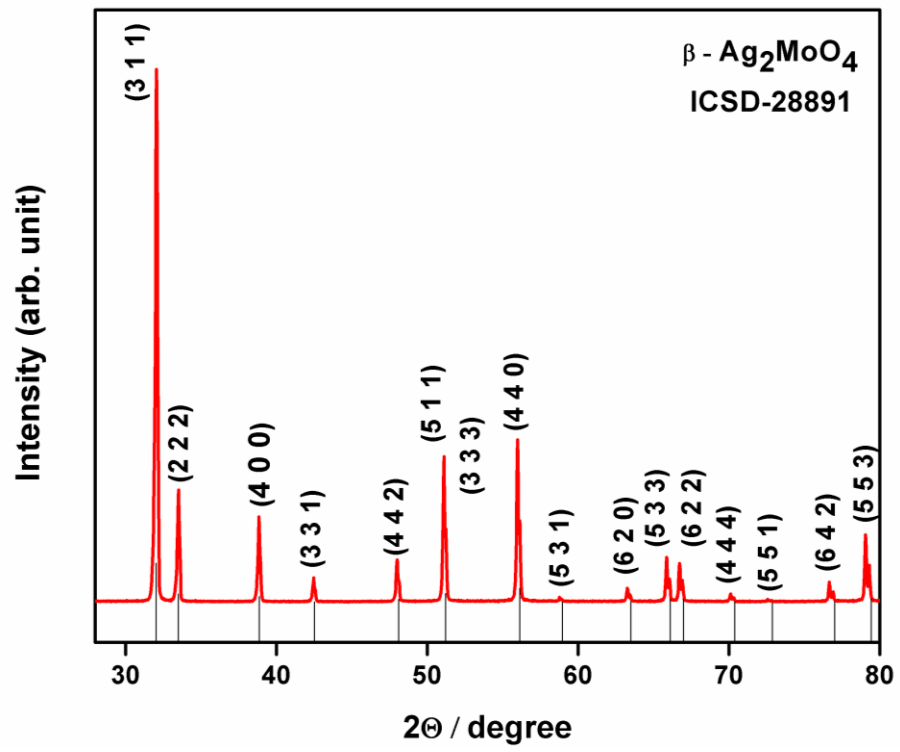

Figure 1: XRD of a β–Ag_2MoO_4 sample.

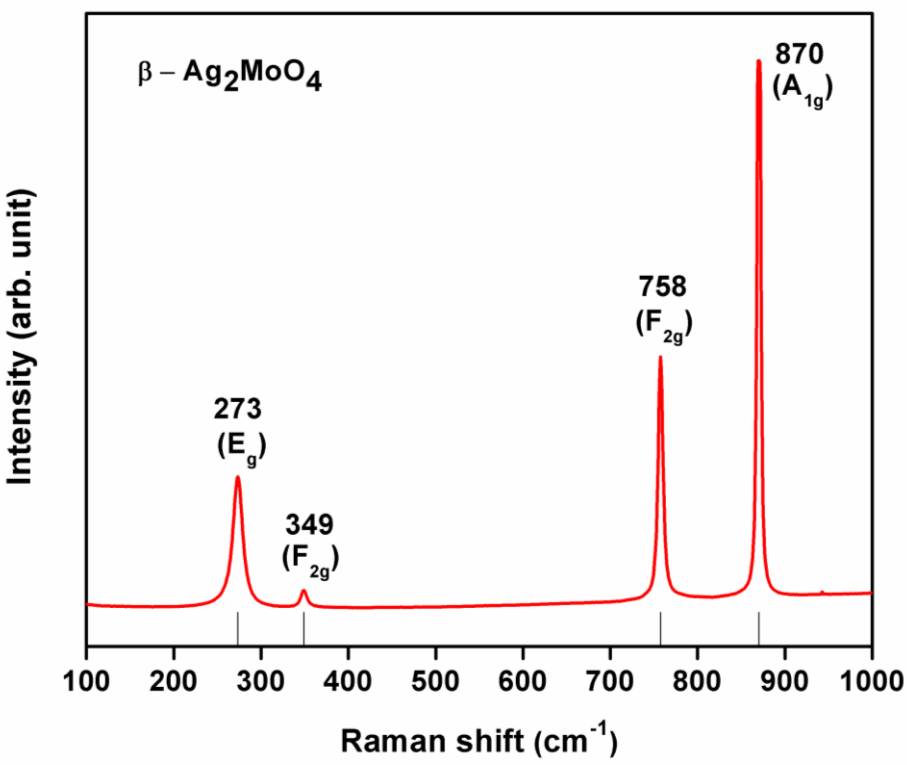

Figure 2: Raman spectrum of β–Ag_2MoO_4.

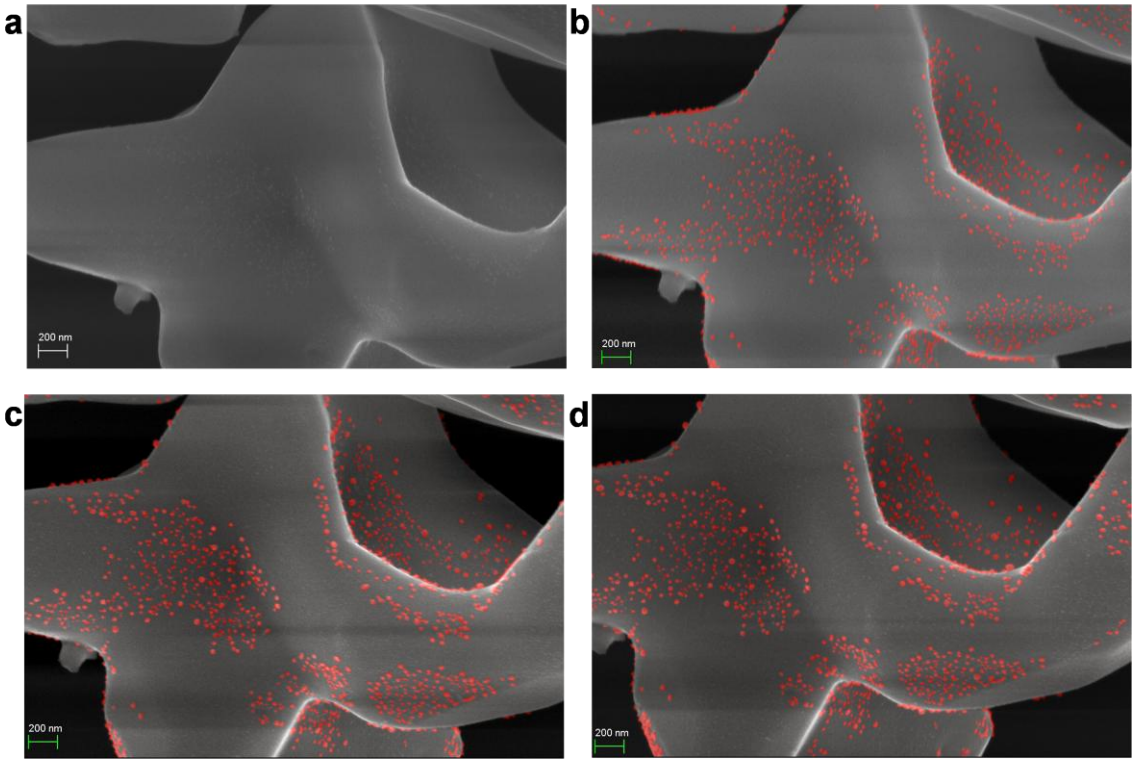

Figure 3: Time-resolved FE-SEM images of β–Ag_2MoO_4.

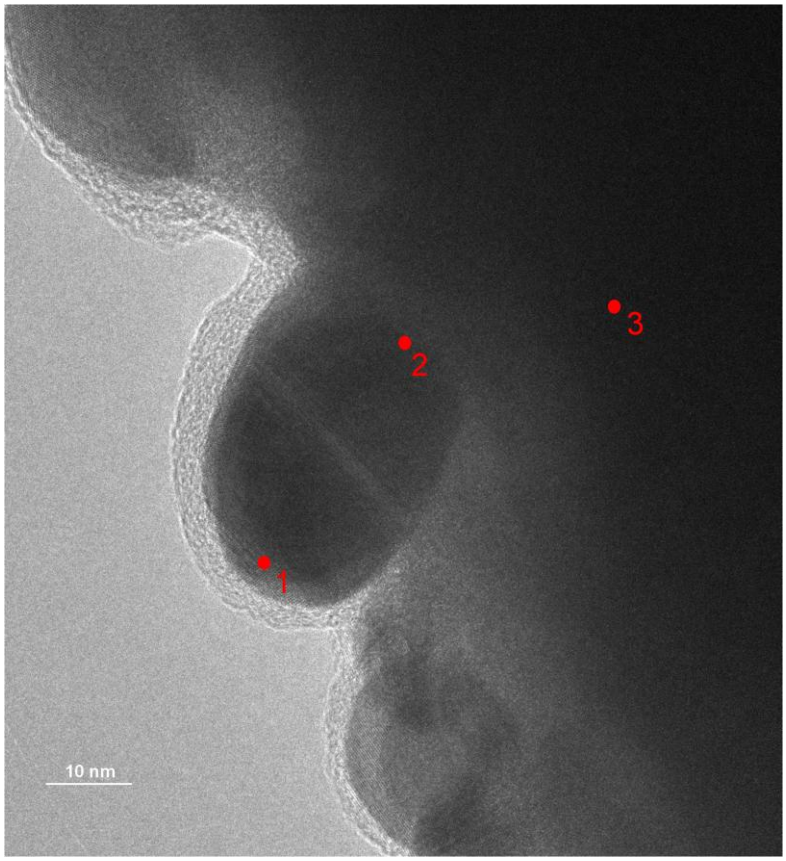

Figure 4: TEM image of β–Ag_2MoO_4.

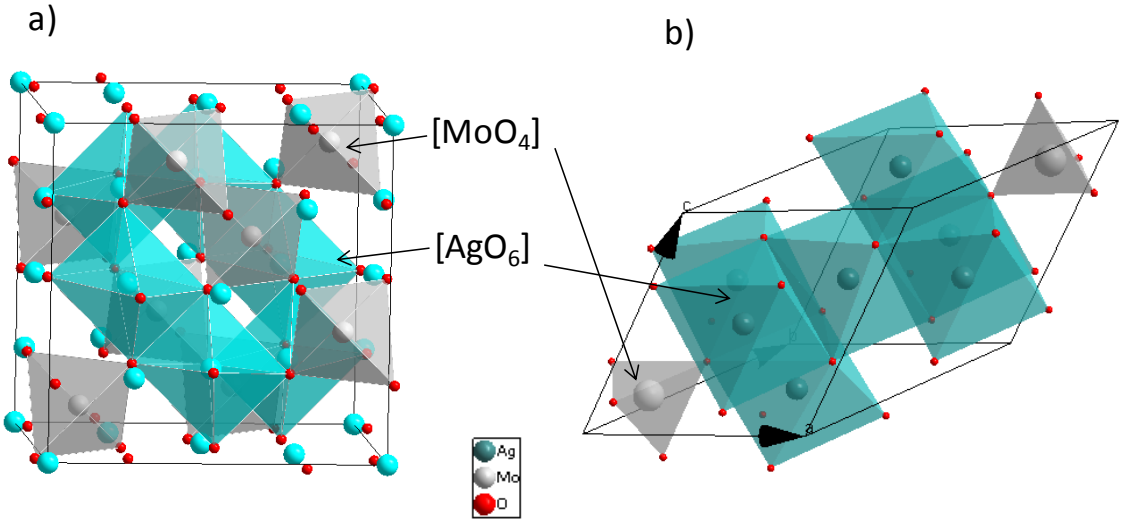

Figure 5: Spinel structure of β-Ag_2MoO_4; a) conventional cell and b) primitive cell.

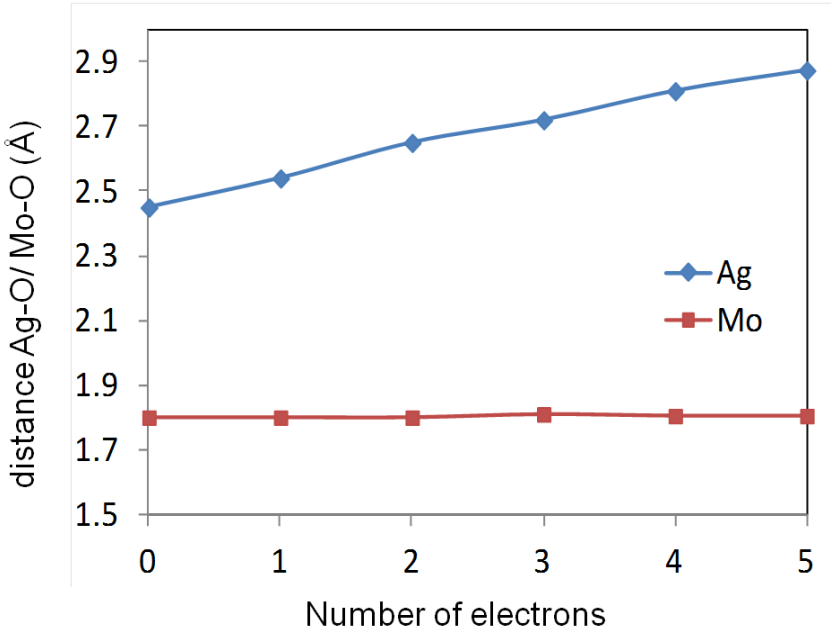

Figure 6: Ag-O and Mo-O distances as a function of the number of electrons added, N.

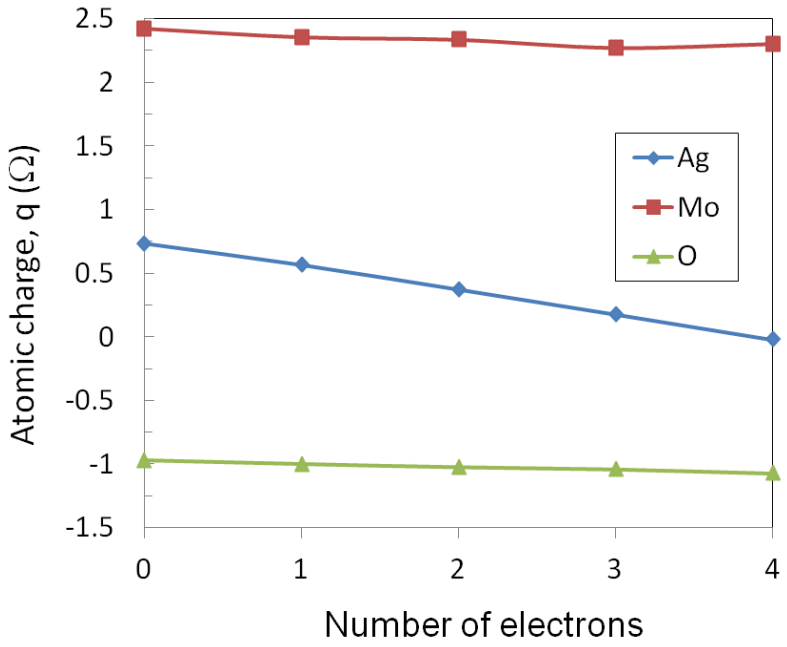

Figure 7: Bader charge density of Ag, Mo and O centers (of $[AgO_6]$ and $[MoO_4]$ clusters) as a function of the number of electrons added. q(Ω) represents the number of valence electrons minus the calculated charge density.

Table 1: Ag and Mo relationship shown by EDS.

Points	Ag(%)	Mo(%)
1	100	0
2	61	38
3	64	36

Table 2.Charge density at the (3,-1) BCPs and its Laplacian in Ag-O bonds for [AgO_6] clusters as a function of the number of electrons added, N.

Ag-O		
N	ρ_{bcp}	$\nabla^2\rho_{bcp}$
0	0.26	3.21
1	0.16	1.93
2	0.11	1.18
3	0.08	0.79
4	0.06	0.61